Oligomer Growth | Hot Paper

DOI: 10.1002/ange.201402309

Controlled Electropolymerization of Ruthenium(II) Vinylbipyridyl Complexes in Mesoporous Nanoparticle Films of TiO_2**

*Zhen Fang, Shahar Keinan, Leila Alibabaei, Hanlin Luo, Akitaka Ito, and Thomas J. Meyer**

Abstract: *Surface-initiated, oligomeric assemblies of ruthenium(II) vinylpolypyridyl complexes have been grown within the cavities of mesoporous nanoparticle films of TiO_2 by electrochemically controlled radical polymerization. Surface growth was monitored by cyclic voltammetry as well as UV/Vis and X-ray photoelectron spectroscopy. Polymerization occurs by a radical chain mechanism following cyclic voltammetry scans to negative potentials where reduction occurs at the π^* levels of the polypyridyl ligands. Oligomeric growth within the cavities of the TiO_2 films occurs until an average of six repeat units are added to the surface-bound initiator site, which is in agreement with estimates of the internal volumes of the pores in the nanoparticle films.*

Surface-bound chromophores, catalysts, and molecular assemblies that are based on ruthenium(II) polypyridyl complexes have been widely used in optoelectronic applications because of their synthetic tunability and desirable physical and chemical properties.[1–5] A highly successful strategy has evolved that is based on linking molecules derivatized with a carboxylic acid (−COOH) or a phosphonic acid ($-P{=}O(OH)_2$) to oxide surfaces. In water, this strategy is limited by surface hydrolysis of the carboxylates, and, for the phosphonates, by surface hydrolysis above pH 7. Far more stable binding has been achieved by an electropolymerization method through reductive electropolymerization based on vinyl-substituted polypyridyl ligands[6,7] or oxidative electropolymerization with pyrrole-containing ligands.[8–11] With two or more vinyl substituents, vinyl polymerization results in the formation of network polymers and precipitation on the electrode surface.[12,13] A combined strategy has been described in which vinyl-derivatized carboxylate or phosphonate complexes are first bound to electrode surfaces, which is followed by the electropolymerization of electroactive or protective overlayer network polymers.[14,15]

A related, electrochemically initiated procedure in solution has been described by Matyjaszewski et al. and is based on the reduction of Cu^{II} complexes to Cu^{I}, with the Cu^{I} species inducing atom-transfer radical polymerization (ATRP) of organic halides.[16] This approach has led to remarkable advances in controlled radical polymerization, which are based on ligand changes to control the redox potential of the $Cu^{II/I}$ initiator.

In negative cyclic voltammetry scans into the π^*(bpy) reduction region (bpy = 2,2′-bipyridine), the Fe^{II} or Ru^{II} tris complexes of 4-bromomethyl-4′-methyl-2,2′-bipyridine (4-Br-4′-Mebpy) or 4,4′-bis(bromomethyl)-2,2′-bipyridine undergo Br^- loss, $-CH_2^{\bullet}$ radical formation, and radical coupling to give linear and 2D metallopolymeric networks.[17]

The combination of initial surface binding, ligand-based reduction with loss of Br^-, and vinyl polymerization suggests a possible approach to controlled vinyl polymerization and oligomer formation on electrode surfaces and in the cavities of nanoparticle oxides. Herein, we describe a novel electrochemical procedure in which surface binding and single vinyl-ligand-based reduction are combined to achieve the stepwise growth of linear chain oligomers from a surface-bound Ru^{II} complex within the cavities of mesoscopic nanoparticle films of TiO_2. This method is based on the reductive initiation of the oligomerization of $[Ru(bpy)_2(4\text{-Me-}4'\text{-vinylbpy})]^{2+}$ (**2**; 4-Me-4′-vinylbpy = 4-vinyl-4′-methyl-2,2′-bipyridine) at surface-bound $[Ru(4,4'\text{-}PO_3H_2\text{-}2,2'\text{-bpy})_2(4\text{-Br-}4'\text{-Mebpy})]^{2+}$ (**1**; 4,4′-PO_3H_2-2,2′-bpy = 4,4′-diphosphonic acid-2,2′-bipyridine).

As shown in Figure 1, the initiator site is surface-bound within the pores of mesoporous TiO_2 films by initial binding of the phosphonate to the surface. This strategy provides an in situ method for stepwise oligomeric growth on the surfaces of metal oxide electrodes and semiconductors with aqueous surface binding stability from the surface phosphonate links. It is a versatile approach in that oligomeric chain growth is controlled by the number of reductive scan cycles. It provides a surface-specific synthetic route for forming controlled molecular structures on any conducting substrate with control of both content and spatial organization. The resulting polychromophoric assemblies, which are bound within the pores of the nanoparticle films of TiO_2, are of interest as possible "antenna" for chromophore–catalyst assemblies, with excitation and rapid intra-strand energy transfer used

[*] Dr. Z. Fang, Dr. S. Keinan, Dr. L. Alibabaei, H. Luo, Prof. Dr. T. J. Meyer
Department of Chemistry
University of North Carolina at Chapel Hill
CB#3209, Chapel Hill, NC 27599-3290 (USA)
E-mail: tjmeyer@unc.edu
Dr. A. Ito
Department of Chemistry, Graduate School of Science
Osaka City University
3-3-138, Sugimoto, Sumiyoshi-ku, Osaka 558-8585 (Japan)

[**] This research was supported primarily by the UNC EFRC: Center for Solar Fuels, an Energy Frontier Research Center funded by the U.S. Department of Energy, Office of Science, Office of Basic Energy Sciences (DE-SC0001011; supporting Z.F., S.K., and L.A.). H.L. is supported by a Royster Society Fellowship at UNC. Support from the U.S. Department of Energy, Office of Science, Office of Basic Energy Sciences (DE-FG02-06ER15788) to A.I. is acknowledged. We thank the Chapel Hill Analytical and Nanofabrication Laboratory for XPS measurements. We also thank Prof. Wenbin Lin for support with the BET measurements.

Supporting information for this article is available on the WWW under http://dx.doi.org/10.1002/anie.201402309.

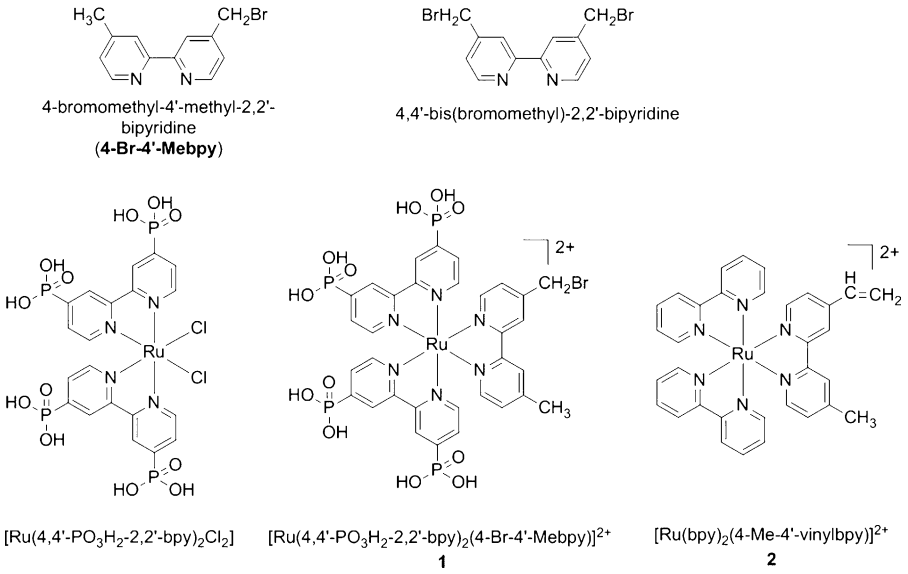

Figure 1. Structures of ligands and complexes.

to sensitize the bound chromophore for excited state electron injection into TiO_2. Facile, intra-strand excited-state energy migration has been observed in related polystyrene-derivatized polymers.[18,19]

$[Ru(4,4'\text{-}PO_3H_2\text{-}2,2'\text{-}bpy)_2(4\text{-}Br\text{-}4'\text{-}Mebpy)]^{2+}$ (**1**) was synthesized as the chloride salt by the reaction between the precursor $[Ru(4,4'\text{-}PO_3H_2\text{-}2,2'\text{-}bpy)_2Cl_2]$ and 4-bromomethyl-4′-methyl-2,2′-bipyridine (Figure 1). Both complexes were prepared by literature procedures.[20,21] Complex formation was monitored by UV/Vis measurements and the shift in the metal-to-ligand charge transfer (MLCT) maximum to 460 nm for **1** (Figure S1). The chloride salt was purified by size-exclusion chromatography on a Sephadex LH-20 column. A resonance at approximately 3.75 ppm appears for the CH_2Br group in the ^1H NMR spectrum of the purified complex in D_2O. The monomer $[Ru(bpy)_2(4\text{-}Me\text{-}4'\text{-}vinylbpy)]^{2+}$ (**2**) was synthesized by a similar procedure, isolated as the chloride salt, and further transformed into the PF_6^- salt by ion exchange through precipitation from a saturated, aqueous ammonium hexafluorophosphate solution.

Complex **1** was adsorbed on nanoparticle (ca. 15 nm) mesoporous films of TiO_2 (ca. 5 μm thick, on fluorine-doped tin oxide (FTO)) by dipping FTO–TiO_2 slides in solutions of the complex (0.2 mM) in $HClO_4$ (0.1 M) for 24 hours to achieve maximum surface coverage. Surface coverages (Γ, in mol cm^{-2}) were determined by visible absorption spectroscopy and the expression $\Gamma = Abs(\lambda) \times \varepsilon(\lambda)/1000$ ($\varepsilon(460\text{ nm}) = 1.56 \times 10^4\text{ M}^{-1}\text{ cm}^{-1}$), where $Abs(\lambda)$ is the absorbance at wavelength λ and $\varepsilon(\lambda)$ the molar extinction coefficient at λ.[22] The maximum surface coverage of approximately 4.8×10^{-8} mol cm^{-2} is consistent with complete surface coverage (Γ_o) with $\Gamma/\Gamma_o \approx 1$.[23] Surface coverage measurements as a function of the concentration of complex in the external solution gave $K_{ad} \approx 1.0 \times 10^4\text{ M}^{-1}$ for the surface binding constant from the Langmuir relationship, $\Gamma = \Gamma_{max}K_{ad}[\mathbf{1}]/(1+K_{ad}[\mathbf{1}])$.

Derivatized TiO_2 films were immersed in acetonitrile solutions of **2** (ca. 1 mM) with $[(n\text{Bu})_4\text{N}]\text{Br}$ (0.1 M) as the supporting electrolyte. A platinum wire was used as the counter electrode and a $AgNO_3$/Ag electrode (0.1M) as the reference ($E = 0.36$ V vs. a saturated calomel electrode (SCE)). In the electropolymerization procedure, the working electrode was scanned from 0 to −2.0 to 0 V for 50 scans at a scan rate of 100 mV s^{-1}. Oligomerization scan cycles were followed by an oxidative scan to 1.4 V, past the surface $Ru^{III/II}$ wave at $E_{1/2} = 0.90$ V, to terminate the reaction. Surface growth was monitored by UV/Vis measurements. Control experiments with bare TiO_2 and with slides coated with $[Ru(4,4'\text{-}PO_3H_2\text{-}2,2'\text{-}bpy)_2(bpy)]^{2+}$ were conducted in parallel.

It has been shown that electropolymerization of $[Ru(4\text{-vinyl-}4'\text{-methyl-}2,2'\text{-bipyridine})_3]^{2+}$ or $[Ru(bpy)_2(4\text{-vinylpyridine})_2]^{2+}$ occurs on a variety of conducting substrates.[24] In contrast, surface electropolymerization of complex **2** with a single vinyl group and no ability for cross-linking is inefficient with a maximum of approximately two layers formed on glassy carbon electrodes after multiple reductive scan cycles. Similarly, following 100 scan cycles with **2** (1 mM) in acetonitrile at TiO_2 (Figure S2), monitoring by UV/Vis spectroscopy revealed a surface coverage of only about 1.6×10^{-8} mol cm^{-2}.

By contrast, for **1** pre-adsorbed on TiO_2 at $\Gamma = 4.8 \times 10^{-8}$ mol cm^{-2}, a series of sequential reductive scan cycles with added **2** resulted in slow oligomeric growth. The results of 50 reductive scan cycles with monitoring by UV/Vis spectroscopy are shown in Figure 2. The absorbance increases gradually with the number of scan cycles until the sixth sequence of 50 scan cycles, which gives a surface coverage of approximately 2.3×10^{-7} mol cm^{-2}. Oligomer formation is accompanied by a shift in the MLCT absorption band maximum from 460 nm to 445 nm. The blue shift is consistent with the addition of **2** to the growing oligomer with its slightly blue-shifted MLCT maximum.

The surface oligomers that result from the stepwise scan procedure are stable indefinitely in cyclic voltammetry (CV) scans through the $Ru^{III/II}$ couple at $E_{1/2} \approx 0.90$ V and bpy-based reduction at −1.65 V. Redox properties remained unchanged even after drying and storing films for two days. Based on the CV results in Figure 3 and the increases in $Ru^{III/II}$ peak current at $E_{1/2} \approx 0.90$ V, on average, 0.8 chromophores were added to the growing oligomer for each sequence of 50 scan cycles with the maximum loading reached after 400 cycles (Supporting Information, Figure S4 and S5). Measurements of the CV current and UV absorbance after 400 scan cycles are consistent with the addition of six units of **2** to the surface-bound complex to give average oligomeric chain lengths of seven Ru^{II} complexes per strand.

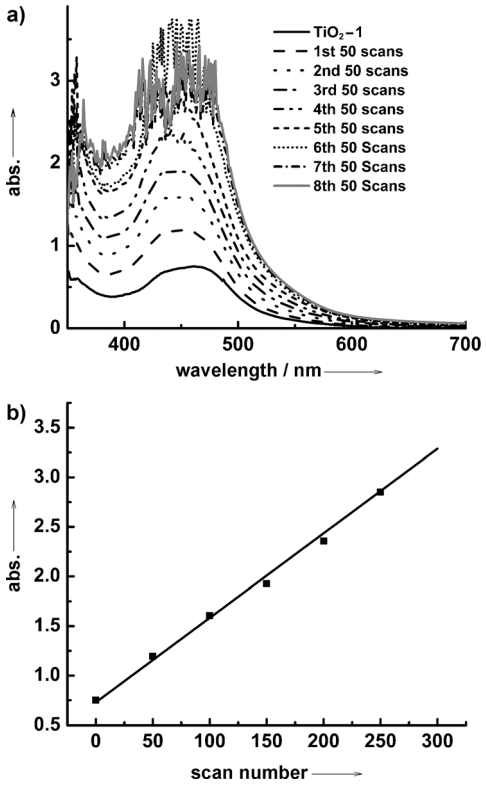

Figure 2. a, b) Absorption spectra (a) and scan-number dependence (b) of **1** pre-adsorbed on TiO_2 at $\Gamma = 4.8 \times 10^{-8}$ mol cm^{-2} on a five micrometer thick mesoporous TiO_2 film following sequential reductive scan cycles: 0→−2.0→0 V, with **2** (1 mM) in $[(n\text{Bu})_4\text{N}]\text{Br}$ (0.1 M) as the supporting electrolyte vs. $AgNO_3$/Ag (0.1 M) in CH_3CN.

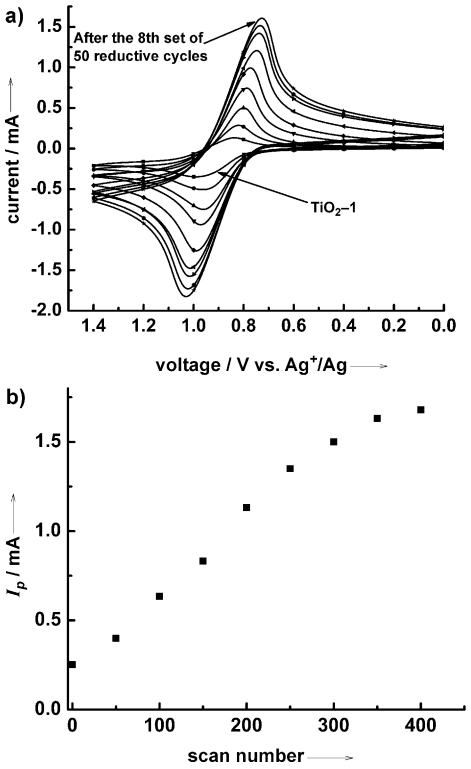

Figure 3. a, b) CVs (a) and scan-number dependence (b) for **1** pre-adsorbed on TiO_2 ($\Gamma = 4.8 \times 10^{-8}$ mol cm^{-2}) after successive 0→−2.0→0 V scan cycles in a solution of **2** (0.1 mM) and $[(n\text{Bu})_4\text{N}]\text{Br}$ (0.1 M) in acetonitrile vs. $AgNO_3$/Ag (0.1 M) in CH_3CN. Monitoring CVs were recorded in fresh acetonitrile solutions of $[(n\text{Bu})_4\text{N}]PF_6$ (0.1 M).

The surface growth of the oligomers was also monitored by X-ray photoelectron spectroscopy (XPS) on dry samples as a function of the number of scan cycles (Figure S6). Figure S6a shows normalized XPS spectra for P 2p and C 1s for **1** pre-absorbed on TiO_2 following 0, 100, 200, and 300 0→−2.0→0 V scan cycles. Oligomeric growth was monitored by increases in the intensities of the characteristic binding energies at approximately 132 and 281 eV for the phosphonate P 2p and Ru $3d_{5/2}$ electrons. There was evidence for bromine in the XPS data, but a broad XPS feature was obtained, as the ionization energies for Br 3d and Ru 4s overlap (Figure S7).[25]

Average internal surface areas in the mesoscopic pores of the TiO_2 films were determined by nitrogen Brunauer—Emmett—Teller (BET) measurements. The results of these measurements revealed that the average pore diameter in the five micrometer thick TiO_2 films was 17.4 nm, which corresponds to an internal cavity radius of 8.7 nm. An estimated pore-size distribution is shown in Figure S8.

The sphere-of-action radius of a $[Ru(bpy)_3]^{2+}$ unit is 0.75 nm.[26] With this quantity and the BET result, an estimate can be made of the average available internal volume in the mesoporous film. Depending on the assumptions made (for calculation details, see the Experimental Section), a close packing of $[Ru(bpy)_3]^{2+}$ spheres for completely filled pore volumes leads to estimates of approximately six $[Ru(bpy)_3]^{2+}$ units attached to each of the 103 surface-bound sites for a low-density assumption, or approximately eight $[Ru(bpy)_3]^{2+}$ units for a high-density or "jammed" assumption. With either estimate, the electro-oligomerization procedure results in nearly completely filled internal volumes in the cavities of the mesoporous films. Packing in the cavities is illustrated in Figure S12, and a drawing of a surface-bound oligomer is shown in Figure S13.

Experimental evidence was obtained for the radical mechanism that is proposed in Figure 4. When the radical trap 2,2,6,6-tetramethylpiperidine-1-oxyl (TEMPO; 0.1M) is added, there is no evidence for oligomeric growth (Figure S9). With added TEMPO, the $E_{1/2}$ value for the $Ru^{III/II}$ wave shifts from 0.88 V to 0.96 V, which is accompanied by a red shift of approximately 8 nm in the visible MLCT λ_{max} value (Figure S10); both observations are consistent with the formation of a TEMPO adduct on the surface.

In the radical mechanism, polymerization is triggered by bpy-based π^* reduction, which triggers Br^- loss, radical formation,[17] C–C coupling, and, with added **2**, oligomerization. Oligomerization is propagated by the monomer in the diffusion layer within the pores of the film. Re-oxidation of oligomer-bound radicals with added Br^- re-establishes a terminal C–Br bond for further propagation cycles. Under our conditions, oligomeric growth on the surface is slow, but highly controllable by choosing the right concentrations and scan rates.

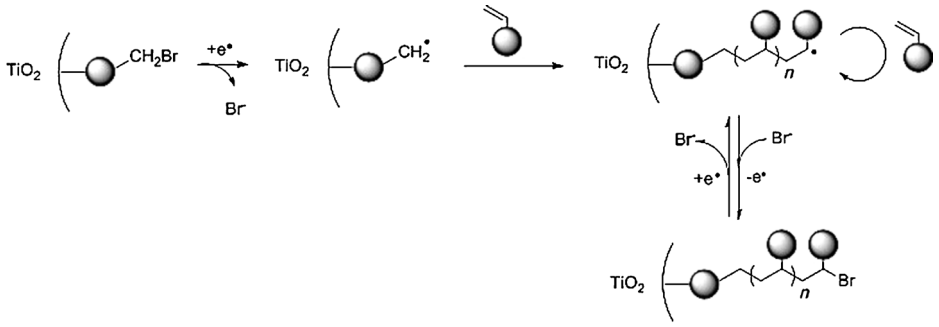

Figure 4. Mechanism of the oligomeric growth of Ru^{II} complexes from **1** in the cavities of the mesoporous TiO_2 film.

The photophysical, electrocatalytic, and device properties of the surface-bound oligomers are currently under investigation. Initial results point towards rapid intra-oligomeric energy transfer. Oligomers grown on ZrO_2, which is inert toward MLCT excited state injection,[27] are strongly emissive (Figure S11), whereas the quenching of the emission on TiO_2 amounts to approximately 90%, which is consistent with the sequence: excitation: TiO_2-Ru^{II}(**1**)-(Ru^{II}(**2**))$_n \xrightarrow{h\nu}$ TiO_2-Ru^{II}(**1**)-(Ru^{II}(**2**)*)(Ru^{II}(**2**))$_{n-1}$; intra-oligomer energy transfer: TiO_2-Ru^{II}(**1**)-(Ru^{II}(**2**)*)(Ru^{II}(**2**))$_{n-1}$ → TiO_2-Ru^{II}(**1**)*-(Ru^{II}(**2**))$_n$; and injection: TiO_2-Ru^{II}(**1**)*-(Ru^{II}(**2**))$_n$ → $TiO_2(e^-)$-Ru^{III}(**1**)-(Ru^{II}(**2**))$_n$.

Experimental Section

Materials: 4′-Methyl-2,2′-bipyridine-4-carbaldehyde, 4-bromomethyl-4′-methyl-2,2′-bipyridine, $[Ru(bpy)_2Cl_2]$, and $[Ru(4,4'\text{-}PO_3H_2\text{-}2,2'\text{-}bpy)_2Cl_2]$ were synthesized according to literature methods.[20,21,28] Methyltriphenylphosphonium iodide (Ph_3PCH_3I), *n*-butyllithium, and ammonium hexafluorophosphate were used as received from Sigma–Aldrich without further purification. Tetrahydrofuran (THF) was refluxed over calcium hydride and distilled. Other solvents were used as received from Fisher Scientific.

Calculation of internal volume: Heptamer-limited electro-oligomerization was investigated by calculating the number of $[Ru(bpy)_3]^{2+}$ units that could fill the cavities of the nanoparticle films with the average pore volume established by the BET measurements. In the first step, we calculated the number of $[Ru(bpy)_3]^{2+}$ spheres that are needed to cover the pore surface. This is a 2D problem, where the most efficient way for circles to pack is in a hexagonal packing pattern of approximately 91% efficiency. Based on the BET measurement, the average pore diameter within the TiO_2 films is 17.4 nm, giving a radius of 8.7 nm. The pore size distribution is shown in Figure S8. The sphere-of-action radius of a $[Ru(bpy)_3]^{2+}$ unit is 0.75 nm.[26] Combining the internal radius of the pores [r(pore) = 8.7–0.75 ≈ 8.0 nm, A(pore) = 804 nm^2] and the $[Ru(bpy)_3]^{2+}$ radius [r($[Ru(bpy)_3]^{2+}$) = 0.75 nm, A($[Ru(bpy)_3]^{2+}$) = 7.1 nm^2] and assuming a packing efficiency of 91% [A(pore, corrected) = 0.91 × 804 nm^2 = 732 nm^2], leads to approximately 103 $[Ru(bpy)_3]^{2+}$ units covering the pore surface.

Hard-sphere balls that are packed irregularly within a container typically form an "irregular" or "jammed" packing structure, which limits further compression. In this structure, the highest density that can be achieved is 63.4%. Combining the radius of the pores [r(pore) = 8.7 nm, V(pore) = 2.758 nm^3] and the $[Ru(bpy)_3]^{2+}$ radius (r($[Ru(bpy)_3]^{2+}$) = 0.75 nm, V($[Ru(bpy)_3]^{2+}$) = 1.8 nm^3] with the 64% packing efficiency [V(pore, corrected) = 0.64 × 2.758 nm^3 = 1.765 nm^3], approximately 980 $[Ru(bpy)_3]^{2+}$ units can fill the pores, with approximately eight $[Ru(bpy)_3]^{2+}$ units attached to each of the 103 surface-bound $[Ru(bpy)_3]^{2+}$ units. At a jamming density of 50%, the pore volume occupied by $[Ru(bpy)_3]^{2+}$ units is smaller [V(pore, corrected) = 0.50 × 2.758 nm^3 = 1.379 nm^3] giving approximately 766 $[Ru(bpy)_3]^{2+}$ units filling the pores with approximately six $[Ru(bpy)_3]^{2+}$ units attached to each of the 103 surface-bound $[Ru(bpy)_3]^{2+}$ sites. The latter number is in agreement with the maximum average oligomeric length that was established experimentally.

Synthesis of 4-methyl-4′-vinyl-2,2′-bipyridine: A suspension of Ph_3PCH_3I (3.67 g, 9.08 mmol) in anhydrous THF (40 mL) was cooled to −78 °C under argon protection. *n*-Butyllithium (5.7 mL, 9.1 mmol) was added dropwise. The mixture was warmed to room temperature and stirred for one hour until a deep-orange solution formed. 4′-Methyl-2,2′-bipyridine-4-carbaldehyde (0.9 g, 4.54 mmol) in anhydrous THF (25 mL) was added in one portion at 0 °C. The mixture was stirred at room temperature overnight. After the reaction was completed, water was added slowly to quench the reaction. The solution was concentrated, extracted with dichloromethane, washed with water, and dried over $MgSO_4$. The solvent was removed under reduced pressure to yield a crude product. The crude product was purified by column chromatography over silica gel using 5:5:1 hexane/CH_2Cl_2/triethylamine as the eluent. After the solution was concentrated, the solid was recrystallized from hexane to yield an orange solid (0.12 g, 23%). ^{1}H NMR ($CDCl_3$, 400 MHz) δ = 8.59 (d, J = 4.00 Hz, 1H), 8.52 (d, J = 4.00 Hz, 1H), 8.38 (s, 1H), 8.22 (s, 1H), 7.43 (d, J = 9.80 Hz, 1H), 7.10 (d, J = 9.80 Hz, 1H), 6.72 (dd, J = 20.00, 8.00 Hz, 1H), 6.05 (d, J = 16.00 Hz, 1H), 5.49 (d, J = 8.00 Hz, 1H), 2.40 ppm (s, 3H). HRMS: m/z calcd for $C_{13}H_{12}N_2^+$: 196.1000 $[M]^+$; found: 196.0993. Elemental analysis calcd (%) for $C_{13}H_{12}N_2$: C 79.56, H 6.16, N 14.27; found: C 79.74, H 6.31, N 14.19.

Synthesis of $[Ru(4,4'\text{-}PO_3H_2\text{-}2,2'\text{-}bpy)_2(4\text{-}Br\text{-}4'\text{-}Mebpy)]Cl_2$ (**1**): A mixture of $[Ru(4,4'\text{-}PO_3H_2\text{-}2,2'\text{-}bpy)_2Cl_2]$ (0.166 g, 0.2 mmol) and 4-bromomethyl-4′-methyl-2,2′-bipyridine (0.052 g, 0.2 mmol) in ethylene glycol (5 mL) was degassed with nitrogen for 30 minutes, then stirred at 120 °C overnight under nitrogen. After cooling down to room temperature, the mixture was poured into acetone (50 mL) to yield a brown precipitate. The crude product was filtered and purified with a Sephadex LH-20 column using water as the eluent. After the water had been removed under reduced pressure, a deep brown solid was obtained (65 mg, 30%). ^{1}H NMR (D_2O, 400 MHz): δ = 8.74–8.50 (m, 5H), 8.38 (m, 2H), 7.89 (s, 4H), 7.68 (s, 1H), 7.55 (s, 4H), 7.33 (s, 1H), 7.22 (s, 1H), 3.75 (br, 2H), 2.52 ppm (s, 3H). HRMS: m/z calcd for $C_{32}H_{31}BrN_6O_{12}P_4Ru^{2+}$: 498.9579 $[M]^{2+}$; found: 498.9600.

Synthesis of $[Ru(bpy)_2(4\text{-}Me\text{-}4'\text{-}vinylbpy)](PF_6)_2$ (**2**): A mixture of $[Ru(bpy)_2Cl_2]$ (0.30 g, 0.61 mmol) and 4-methyl-4′-vinyl-2,2′-bipyridine (0.12 g, 0.61 mmol) in ethanol (5 mL) and water (5 mL) was degassed with nitrogen for 30 minutes. The mixture was heated at reflux for 3 h under nitrogen protection. Ethanol was removed by distillation under reduced pressure. The unreacted solid was filtered and washed with water. The water solution was concentrated. To this solution, NH_4PF_6 (0.2 g) was added to yield a deep-orange solid. Having been washed with cold water, the solid was dried under vacuum (0.28 g, 67%). ^{1}H NMR (CD_3CN, 400 MHz): δ = 8.51 (d, J = 16.00 Hz, 4H), 8.41 (s, 1H), 8.04–8.00 (m, 4H), 7.84–7.81 (m, 4H), 7.70 (d, J = 8.00 Hz, 1H), 7.61 (d, J = 8.00 Hz, 1H), 7.35–7.31 (m, 6H), 7.21 (d, J = 4.00 Hz, 1H), 6.89 (dd, J = 20.00, 12.00 Hz, 1H), 6.21 (d,

$J = 10.00$ Hz, 1H), 5.68 (d, $J = 12.00$ Hz, 1H), 2.52 ppm (s, 3H). HRMS: m/z calcd for $C_{33}H_{28}N_6Ru^{2+}$: 305.0710 $[M]^{2+}$; found: 305.0699.

Received: February 11, 2014
Published online: March 28, 2014

Keywords: mesoporous materials · oligomers · reductive polymerization · ruthenium · TiO_2 films

[1] S. M. Borisov, O. S. Wolfbeis, *Chem. Rev.* **2008**, *108*, 423 – 461.
[2] K. Szaciłowski, W. Macyk, A. Drzewiecka-Matuszek, M. Brindell, G. Stochel, *Chem. Rev.* **2005**, *105*, 2647 – 2694.
[3] F. Loiseau, F. Nastasi, A. M. Stadler, S. Campagna, J. M. Lehn, *Angew. Chem.* **2007**, *119*, 6256 – 6259; *Angew. Chem. Int. Ed.* **2007**, *46*, 6144 – 6147.
[4] M. W. Cooke, G. S. Hanan, F. Loiseau, S. Campagna, M. Watanabe, Y. Tanaka, *J. Am. Chem. Soc.* **2007**, *129*, 10479 – 10488.
[5] D. W. Thompson, A. Ito, T. J. Meyer, *Pure Appl. Chem.* **2013**, *85*, 1257 – 1305.
[6] M. C. E. Bandeira, J. A. Crayston, C. V. Franco, A. Glidle, *Phys. Chem. Chem. Phys.* **2007**, *9*, 1003 – 1012.
[7] S. C. Paulson, S. A. Sapp, C. Michael Elliott, *J. Phys. Chem. B* **2001**, *105*, 8718 – 8724.
[8] K. C. Cheung, P. Guo, M. H. So, Z. Y. Zhou, L. Y. S. Lee, K. Y. Wong, *Inorg. Chem.* **2012**, *51*, 6468 – 6475.
[9] M. Buda, J. C. Moutet, A. Pailleret, E. Saint-Aman, R. Ziessel, *J. Electroanal. Chem.* **2000**, *484*, 164 – 171.
[10] S. Harmar-Thibault, J. C. Mouter, S. Tingry, *J. Organomet. Chem.* **1997**, *532*, 31 – 37.
[11] M. A. Carvalho de Medeiros, S. Cosnier, A. Deronzier, J. C. Moutet, *Inorg. Chem.* **1996**, *35*, 2659 – 2664.
[12] J. A. Moss, R. Argazzi, C. A. Bignozzi, T. J. Meyer, *Inorg. Chem.* **1997**, *36*, 762 – 763.
[13] D. A. Torelli, D. P. Harrison, A. M. Lapides, T. J. Meyer, *ACS Appl. Mater. Interfaces* **2013**, *5*, 7050 – 7057.
[14] J. A. Moss, J. C. Yang, J. M. Stipkala, X. Wen, C. A. Bignozzi, G. J. Meyer, T. J. Meyer, *Inorg. Chem.* **2004**, *43*, 1784 – 1792.
[15] A. M. Lapides, D. L. Ashford, K. Hanson, D. A. Torelli, J. L. Templeton, T. J. Meyer, *J. Am. Chem. Soc.* **2013**, *135*, 15450 – 15458.
[16] A. J. D. Magenau, N. C. Strandwitz, A. Gennaro, K. Matyjaszewski, *Science* **2011**, *332*, 81 – 84.
[17] S. Gould, G. F. Strouse, T. J. Meyer, B. P. Sullivan, *Inorg. Chem.* **1991**, *30*, 2942 – 2949.
[18] L. M. Dupray, M. Devenney, D. R. Striplin, T. J. Meyer, *J. Am. Chem. Soc.* **1997**, *119*, 10243 – 10244.
[19] M. H. V. Huynh, D. M. Dattelbaum, T. J. Meyer, *Coord. Chem. Rev.* **2005**, *249*, 457 – 483.
[20] M. R. Norris, J. J. Concepcion, C. R. K. Glasson, Z. Fang, A. M. Lapides, D. L. Ashford, J. L. Templeton, T. J. Meyer, *Inorg. Chem.* **2013**, *52*, 12492 – 12501.
[21] K. E. Berg, A. Tran, M. K. Raymond, M. Abrahamsson, J. Wolny, S. Redon, M. Andersson, L. Sun, S. Styring, L. Hammarstrom, H. Toftlund, B. Akermark, *Eur. J. Inorg. Chem.* **2001**, 1019 – 1029.
[22] L. A. Gallagher, S. A. Serron, X. Wen, B. J. Hornstein, D. M. Dattelbaum, J. R. Schoonover, T. J. Meyer, *Inorg. Chem.* **2005**, *44*, 2089 – 2097.
[23] K. Hanson, M. K. Brennaman, A. Ito, H. Luo, W. Song, K. A. Parker, R. Ghosh, M. R. Norris, C. R. K. Glasson, J. J. Concepcion, R. Lopez, T. J. Meyer, *J. Phys. Chem. C* **2012**, *116*, 14837 – 14847.
[24] P. Denisevich, H. D. Abruna, C. R. Leinner, T. J. Meyer, R. W. Murray, *Inorg. Chem.* **1982**, *21*, 2153 – 2161.
[25] R. Spohr, T. Bergmark, N. Magnusson, L. O. Werme, C. Nordling, K. Siegbahn, *Phys. Scr.* **1970**, *2*, 31 – 37.
[26] A. A. Martí, J. L. Colón, *Inorg. Chem.* **2010**, *49*, 7298 – 7303.
[27] R. Katoh, A. Furube, T. Yoshihara, K. Hara, G. Fujihashi, S. Takano, S. Murata, H. Arakawa, M. Tachiya, *J. Phys. Chem. B* **2004**, *108*, 4818 – 4822.
[28] B. M. Peek, G. T. Ross, S. W. Edwards, G. J. Meyer, T. J. Meyer, B. W. Erickson, *Int. J. Pept. Protein Res.* **1991**, *38*, 114 – 123.